Centrality dependence of $\pi^{+/-}$, $K^{+/-}$, p and $\overline{p}$ production from $\sqrt{s_{NN}} = 130$ GeV Au + Au Collisions at RHIC

K. Adcox,[40] S.S. Adler,[3] N.N. Ajitanand,[27] Y. Akiba,[14] J. Alexander,[27] L. Aphecetche,[34] Y. Arai,[14] S.H. Aronson,[3] R. Averbeck,[28] T.C. Awes,[29] K.N. Barish,[5] P.D. Barnes,[19] J. Barrette,[21] B. Bassalleck,[25] S. Bathe,[22] V. Baublis,[30] A. Bazilevsky,[12,32] S. Belikov,[12,13] F.G. Bellaiche,[29] S.T. Belyaev,[16] M.J. Bennett,[19] Y. Berdnikov,[35] S. Botelho,[33] M.L. Brooks,[19] D.S. Brown,[26] N. Bruner,[25] D. Bucher,[22] H. Buesching,[22] V. Bumazhnov,[12] G. Bunce,[3,32] J. Burward-Hoy,[28] S. Butsyk,[28,30] T.A. Carey,[19] P. Chand,[2] J. Chang,[5] W.C. Chang,[1] L.L. Chavez,[25] S. Chernichenko,[12] C.Y. Chi,[8] J. Chiba,[14] M. Chiu,[8] R.K. Choudhury,[2] T. Christ,[28] T. Chujo,[3,39] M.S. Chung,[15,19] P. Chung,[27] V. Cianciolo,[29] B.A. Cole,[8] D.G. D'Enterria,[34] G. David,[3] H. Delagrange,[34] A. Denisov,[12] A. Deshpande,[32] E.J. Desmond,[3] O. Dietzsch,[33] B.V. Dinesh,[2] A. Drees,[28] A. Durum,[12] D. Dutta,[2] K. Ebisu,[24] Y.V. Efremenko,[29] K. El Chenawi,[40] H. En'yo,[17,31] S. Esumi,[39] L. Ewell,[3] T. Ferdousi,[5] D.E. Fields,[25] S.L. Fokin,[16] Z. Fraenkel,[42] A. Franz,[3] A.D. Frawley,[9] S.-Y. Fung,[5] S. Garpman,[20] T.K. Ghosh,[40] A. Glenn,[36] A.L. Godoi,[33] Y. Goto,[32] S.V. Greene,[40] M. Grosse Perdekamp,[32] S.K. Gupta,[2] W. Guryn,[3] H.-Å. Gustafsson,[20] J.S. Haggerty,[3] H. Hamagaki,[7] A.G. Hansen,[19] H. Hara,[24] E.P. Hartouni,[18] R. Hayano,[38] N. Hayashi,[31] X. He,[10] T.K. Hemmick,[28] J.M. Heuser,[28] M. Hibino,[41] J.C. Hill,[13] D.S. Ho,[43] K. Homma,[11] B. Hong,[15] A. Hoover,[26] T. Ichihara,[31,32] K. Imai,[17,31] M.S. Ippolitov,[16] M. Ishihara,[31,32] B.V. Jacak,[28,32] W.Y. Jang,[15] J. Jia,[28] B.M. Johnson,[3] S.C. Johnson,[18,28] K.S. Joo,[23] S. Kametani,[41] J.H. Kang,[43] M. Kann,[30] S.S. Kapoor,[2] S. Kelly,[8] B. Khachaturov,[42] A. Khanzadeev,[30] J. Kikuchi,[41] D.J. Kim,[43] H.J. Kim,[43] S.Y. Kim,[43] Y.G. Kim,[43] W.W. Kinnison,[19] E. Kistenev,[3] A. Kiyomichi,[39] C. Klein-Boesing,[22] S. Klinksiek,[25] L. Kochenda,[30] V. Kochetkov,[12] D. Koehler,[25] T. Kohama,[11] D. Kotchetkov,[5] A. Kozlov,[42] P.J. Kroon,[3] K. Kurita,[31,32] M.J. Kweon,[15] Y. Kwon,[43] G.S. Kyle,[26] R. Lacey,[27] J.G. Lajoie,[13] J. Lauret,[27] A. Lebedev,[13,16] D.M. Lee,[19] M.J. Leitch,[19] X.H. Li,[5] Z. Li,[6,31] D.J. Lim,[43] M.X. Liu,[19] X. Liu,[6] Z. Liu,[6] C.F. Maguire,[40] J. Mahon,[3] Y.I. Makdisi,[3] V.I. Manko,[16] Y. Mao,[6,31] S.K. Mark,[21] S. Markacs,[8] G. Martinez,[34] M.D. Marx,[28] A. Masaike,[17] F. Matathias,[28] T. Matsumoto,[7,41] P.L. McGaughey,[19] E. Melnikov,[12] M. Merschmeyer,[22] F. Messer,[28] M. Messer,[3] Y. Miake,[39] T.E. Miller,[40] A. Milov,[42] S. Mioduszewski,[3,36] R.E. Mischke,[19] G.C. Mishra,[10] J.T. Mitchell,[3] A.K. Mohanty,[2] D.P. Morrison,[3] J.M. Moss,[19] F. Mühlbacher,[28] M. Muniruzzaman,[5] J. Murata,[31] S. Nagamiya,[14] Y. Nagasaka,[24] J.L. Nagle,[8] Y. Nakada,[17] B.K. Nandi,[5] J. Newby,[36] L. Nikkinen,[21] P. Nilsson,[20] S. Nishimura,[7] A.S. Nyanin,[16] J. Nystrand,[20] E. O'Brien,[3] C.A. Ogilvie,[13] H. Ohnishi,[3,11] I.D. Ojha,[4,40] M. Ono,[39] V. Onuchin,[12] A. Oskarsson,[20] L. Österman,[20] I. Otterlund,[20] K. Oyama,[7,38] L. Paffrath,[3,*] A.P.T. Palounek,[19] V.S. Pantuev,[28] V. Papavassiliou,[26] S.F. Pate,[26] T. Peitzmann,[22] A.N. Petridis,[13] C. Pinkenburg,[3,27] R.P. Pisani,[3] P. Pitukhin,[12] F. Plasil,[29] M. Pollack,[28,36] K. Pope,[36] M.L. Purschke,[3] I. Ravinovich,[42] K.F. Read,[29,36] K. Reygers,[22] V. Riabov,[30,35] Y. Riabov,[30] M. Rosati,[13] A.A. Rose,[40] S.S. Ryu,[43] N. Saito,[31,32] A. Sakaguchi,[11] T. Sakaguchi,[7,41] H. Sako,[39] T. Sakuma,[31,37] V. Samsonov,[30] T.C. Sangster,[18] R. Santo,[22] H.D. Sato,[17,31] S. Sato,[39] S. Sawada,[14] B.R. Schlei,[19] Y. Schutz,[34] V. Semenov,[12] R. Seto,[5] T.K. Shea,[3] I. Shein,[12] T.-A. Shibata,[31,37] K. Shigaki,[14] T. Shiina,[19] Y.H. Shin,[43] I.G. Sibiriak,[16] D. Silvermyr,[20] K.S. Sim,[15] J. Simon-Gillo,[19] C.P. Singh,[4] V. Singh,[4] M. Sivertz,[3] A. Soldatov,[12] R.A. Soltz,[18] S. Sorensen,[29,36] P.W. Stankus,[29] N. Starinsky,[21] P. Steinberg,[8] E. Stenlund,[20] A. Ster,[44] S.P. Stoll,[3] M. Sugioka,[31,37] T. Sugitate,[11] J.P. Sullivan,[19] Y. Sumi,[11] Z. Sun,[6] M. Suzuki,[39] E.M. Takagui,[33] A. Taketani,[31] M. Tamai,[41] K.H. Tanaka,[14] Y. Tanaka,[24] E. Taniguchi,[31,37] M.J. Tannenbaum,[3] J. Thomas,[28] J.H. Thomas,[18] T.L. Thomas,[25] W. Tian,[6,36] J. Tojo,[17,31] H. Torii,[17,31] R.S. Towell,[19] I. Tserruya,[42] H. Tsuruoka,[39] A.A. Tsvetkov,[16] S.K. Tuli,[4] H. Tydesjö,[20] N. Tyurin,[12] T. Ushiroda,[24] H.W. van Hecke,[19] C. Velissaris,[26] J. Velkovska,[28] M. Velkovsky,[28] A.A. Vinogradov,[16] M.A. Volkov,[16] A. Vorobyov,[30] E. Vznuzdaev,[30] H. Wang,[5] Y. Watanabe,[31,32] S.N. White,[3] C. Witzig,[3] F.K. Wohn,[13] C.L. Woody,[3] W. Xie,[5,42] K. Yagi,[39] S. Yokkaichi,[31] G.R. Young,[29] I.E. Yushmanov,[16] W.A. Zajc,[8] Z. Zhang,[28] and S. Zhou[6]

(PHENIX Collaboration)

[1] *Institute of Physics, Academia Sinica, Taipei 11529, Taiwan*

[2] *Bhabha Atomic Research Centre, Bombay 400 085, India*

[3] *Brookhaven National Laboratory, Upton, NY 11973-5000, USA*

[4] *Department of Physics, Banaras Hindu University, Varanasi 221005, India*

[5] *University of California - Riverside, Riverside, CA 92521, USA*

[6] *China Institute of Atomic Energy (CIAE), Beijing, People's Republic of China*

[7] *Center for Nuclear Study, Graduate School of Science, University of Tokyo, 7-3-1 Hongo, Bunkyo, Tokyo 113-0033, Japan*

[8] *Columbia University, New York, NY 10027 and Nevis Laboratories, Irvington, NY 10533, USA*

[9] *Florida State University, Tallahassee, FL 32306, USA*

[10] *Georgia State University, Atlanta, GA 30303, USA*

[11] *Hiroshima University, Kagamiyama, Higashi-Hiroshima 739-8526, Japan*

[12] Institute for High Energy Physics (IHEP), Protvino, Russia
[13] Iowa State University, Ames, IA 50011, USA
[14] KEK, High Energy Accelerator Research Organization, Tsukuba-shi, Ibaraki-ken 305-0801, Japan
[15] Korea University, Seoul, 136-701, Korea
[16] Russian Research Center "Kurchatov Institute", Moscow, Russia
[17] Kyoto University, Kyoto 606, Japan
[18] Lawrence Livermore National Laboratory, Livermore, CA 94550, USA
[19] Los Alamos National Laboratory, Los Alamos, NM 87545, USA
[20] Department of Physics, Lund University, Box 118, SE-221 00 Lund, Sweden
[21] McGill University, Montreal, Quebec H3A 2T8, Canada
[22] Institut für Kernphysik, University of Münster, D-48149 Münster, Germany
[23] Myongji University, Yongin, Kyonggido 449-728, Korea
[24] Nagasaki Institute of Applied Science, Nagasaki-shi, Nagasaki 851-0193, Japan
[25] University of New Mexico, Albuquerque, NM 87131, USA
[26] New Mexico State University, Las Cruces, NM 88003, USA
[27] Chemistry Department, State University of New York - Stony Brook, Stony Brook, NY 11794, USA
[28] Department of Physics and Astronomy, State University of New York - Stony Brook, Stony Brook, NY 11794, USA
[29] Oak Ridge National Laboratory, Oak Ridge, TN 37831, USA
[30] PNPI, Petersburg Nuclear Physics Institute, Gatchina, Russia
[31] RIKEN (The Institute of Physical and Chemical Research), Wako, Saitama 351-0198, JAPAN
[32] RIKEN BNL Research Center, Brookhaven National Laboratory, Upton, NY 11973-5000, USA
[33] Universidade de São Paulo, Instituto de Física, Caixa Postal 66318, São Paulo CEP05315-970, Brazil
[34] SUBATECH (Ecole des Mines de Nantes, IN2P3/CNRS, Universite de Nantes) BP 20722 - 44307, Nantes-cedex 3, France
[35] St. Petersburg State Technical University, St. Petersburg, Russia
[36] University of Tennessee, Knoxville, TN 37996, USA
[37] Department of Physics, Tokyo Institute of Technology, Tokyo, 152-8551, Japan
[38] University of Tokyo, Tokyo, Japan
[39] Institute of Physics, University of Tsukuba, Tsukuba, Ibaraki 305, Japan
[40] Vanderbilt University, Nashville, TN 37235, USA
[41] Waseda University, Advanced Research Institute for Science and Engineering, 17 Kikui-cho, Shinjuku-ku, Tokyo 162-0044, Japan
[42] Weizmann Institute, Rehovot 76100, Israel
[43] Yonsei University, IPAP, Seoul 120-749, Korea
[44] KFKI Research Institute for Particle and Nuclear Physics (RMKI), Budapest, Hungary†
(December 17, 2001)

Identified $\pi^{+/-}$, $K^{+/-}$, p and $\overline{p}$ transverse momentum spectra at mid-rapidity in $\sqrt{s_{NN}}$ = 130 GeV Au-Au collisions were measured by the PHENIX experiment at RHIC as a function of collision centrality. Average transverse momenta increase with the number of participating nucleons in a similar way for all particle species. The multiplicity densities scale faster than the number of participating nucleons. Kaon and nucleon yields per participant increase faster than the pion yields. In central collisions at high transverse momenta ($p_T \gtrsim 2$ GeV/c), anti-proton and proton yields are comparable to the pion yields.

PACS numbers: 25.75.Dw

We report first results on identified pion, kaon, proton, and anti-proton production as a function of collision centrality in $\sqrt{s_{NN}}$ = 130 GeV Au+Au collisions, measured in the PHENIX experiment during the first run of the Relativistic Heavy Ion Collider (RHIC) in year 2000. The new experimental heavy ion program is dedicated to studying nuclear matter in extreme conditions. The PHENIX objective is to search for signatures of deconfinement and chiral symmetry restoration and to study the transition from normal to deconfined nuclear matter by utilizing a wide variety of probes.

Early RHIC results show that the transverse energy density and the particle multiplicities are considerably higher than previously observed in relativistic heavy-ion collisions [1–3]. The measured energy densities extend into the region predicted to be favorable for the formation of a quark-gluon plasma. Identified hadron spectroscopy provides a tool for studying the reaction dynamics beyond that of global event characterization. The yields of hadrons reflect the particle production mechanism, while the spectral shapes are sensitive to the dynamical evolution of the system. The mass and centrality dependence of the spectra can help to differentiate between competing theoretical descriptions such as collective hy-

drodynamical expansion [4,5] or transverse momentum (p_T) broadening in the partonic stage of the reaction [6]. Additionally the relative yields of baryons and mesons at high p_T (> 2 GeV/c) may give insight into the baryon number transport [7] and the interplay between soft and hard processes.

The PHENIX detector has diverse particle identification (PID) capabilities [8], including excellent hadron identification over a broad momentum range. This measurement was performed using a portion of the east central-arm spectrometer, covering pseudo-rapidity $|\eta| < 0.35$ and $\Delta\phi = \pi/4$ in azimuthal angle.

The collision z-vertex position and the timing system's start signal are generated by the Beam-Beam Counters (BBC), which are comprised of two arrays of quartz Cherenkov radiators, surrounding the beam axis in the pseudo-rapidity region $\eta = \pm(3.0 - 3.9)$. The tracking system includes a multi-layer focusing drift chamber located outside an axially-symmetric magnetic field at a radial distance between 2.0 m and 2.4 m followed by a multi-wire proportional chamber with pixel-pad readout (PC1) [9]. Pattern recognition in the DC is based on a combinatorial Hough transform in the track bend plane. The polar angle of the track is determined by PC1 and the location of the collision z-vertex. A track model based on a field-integral look-up table determines the charged particle momentum and the path length to the time-of-flight (TOF) wall. The momentum resolution is $\delta p/p \simeq 0.6\% \oplus 3.6\%\ p$ (GeV/c).

The timing system stop signal for each particle is measured by the TOF scintillator wall, located at a radial distance of 5.06 m resulting in a flight-time measurement with a resolution of $\sigma \simeq 115$ ps. Reconstructed tracks are projected to the TOF and matched with hits in the scintillator slats using a momentum-dependent search window determined by multiple scattering and the momentum resolution. A velocity dependent energy loss cut based on a Bethe-Bloch parameterization is applied to the measured TOF pulse height. Combining the momentum and flight time, we reconstruct the particle mass and select particles by applying 2σ momentum dependent cuts in mass-squared.

Corrections for geometrical acceptance, decay-in-flight, momentum resolution and reconstruction efficiency are determined using a single-particle full GEANT Monte Carlo (MC) simulation. The acceptance correction assumes that the spectra are flat in azimuth and in rapidity for $|y| < 0.5$ [10]. Fiducial area cuts, energy loss and hit-track matching cuts are applied consistently in simulation and data. In peripheral events, the track reconstruction efficiency is $\approx 98\%$. As the centrality increases, the efficiency is reduced due to the increased detector occupancy. Multiplicity dependent corrections are obtained by embedding simulated tracks into real events. Track-by-track corrections are applied taking into account the event centrality and the particle species. The efficiency for pions in the most central events is $\approx (68 \pm 6)\%$, independent of momentum. In the case of overlapping hits in the TOF scintillator slats, the earliest pulse reaching each PMT is recorded. This favors the faster particles; hence, in central events heavier particles suffer an additional reconstruction inefficiency of $\approx 4\%$. Corrections for feed-down from weak decays are not applied. A MC simulation is used to estimate the probability for reconstructing protons from Λ decays as prompt protons. Within the PHENIX acceptance this probability is $\approx 32\%$ at $p_T = 1\,\mathrm{GeV/c}$ and $\approx 12\%$ at $p_T \geq 2\,\mathrm{GeV/c}$. Taking $\frac{\Lambda}{p} = 1$ as an upper limit, we estimate $\approx 24\%$ as the upper limit of weak decay contribution to the reported proton and anti-proton yields.

About 140,000 minimum bias events, representing $92 \pm 4\%$ of the total inelastic cross-section of 6.8 b [1] were analyzed. This sample was subdivided into five centrality classes: $0 - 5\%$, $5 - 15\%$, $15 - 30\%$, $30 - 60\%$ and $60 - 92\%$, using the BBC and Zero-Degree-Calorimeters for event characterization [1]. For each class, the average number of nucleons participating in the collision (N_{part}) is obtained from a Glauber model calculation [11].

Fig. 1 shows the invariant yield as a function of p_T for π^+, K^+, p (left panel) and $\pi^-, K^-, \overline{p}$ (right panel) for three centrality selections. The error bars in the figure are the combined statistical errors in the data and the corrections. The systematic uncertainties from acceptance, multiplicity-dependent efficiency corrections and PID cuts result in an overall systematic uncertainty in the absolute normalization of $\approx 11\%$ for all particles species. As a consistency check, we have added all identified charged hadron spectra in the p_T region where PID is available for all species and compared to the PHENIX charged hadron measurement [11]. The results agree to better than 10% for all centralities. Additionally, the PHENIX π^0 spectra [11] and the charged pion spectra in the region of overlapping p_T are within $\approx 10\%$ for the central and $\approx 25\%$ for the peripheral selections, which is within the systematic errors of the two measurements.

In peripheral events the pion spectra exhibit a concave shape, well described by a power-law parameterization as observed in hadron-hadron collisions [12]. With increasing centrality the curvature in the spectra decreases, leading to an almost exponential dependence on p_T for the most central events. Over the measured p_T range, the kaon spectra can be described by an exponential distribution either in p_T or in $m_T = \sqrt{p_T^2 + m^2}$, while the p and $\overline{p}$ spectra can be described either as a Boltzmann or an exponential distribution in m_T. The slopes of the m_T spectra flatten and the mean transverse momentum ($<p_T>$) increases with particle mass and with centrality. This behavior has been previously observed in lower energy heavy ion collisions at the BNL-AGS [13] and at the CERN-SPS [14,15] and was attributed to collective radial motion (flow) in the rapidly expanding system.

At lower energies, it is not uncommon for the pro-

ton yields to equal or exceed the π^+ yields, since many of the protons come from the initial state. A new feature observed for the first time at RHIC is that in central collisions at $p_T \approx 2\,\mathrm{GeV/c}$ the anti-proton yields are comparable to the negative pion yields. Positive and negative hadrons behave in a similar way. In central events the proton yields approach the π^+ spectra around $p_T \simeq 1.6\,\mathrm{GeV/c}$. As the centrality decreases, this happens at larger p_T. In peripheral events, both the proton and the anti-proton spectra are below the pion spectra in the whole measured p_T range. Since anti-protons are not as numerous as the protons, $\overline{p}$ and π^- yields become comparable only at the high end of the measured pion p_T range in the most central collisions. We note that in pp [16] and $p\overline{p}$ [17] collisions at $\sqrt{s} = 23-63\,\mathrm{GeV}$ and $\sqrt{s} = 300-1800\,\mathrm{GeV}$ respectively, the $\overline{p}/\pi^-$ ratio steadily increases with p_T up to $\simeq 0.33$ at $p_T \simeq 1.5\,\mathrm{GeV/c}$ nearly independent of $\sqrt{s}$. Data on baryon/meson ratios at higher p_T are only available from pp collisions at ISR energies ($\sqrt{s} = 23-63\,\mathrm{GeV}$) and show that above $p_T \simeq 1.5\,\mathrm{GeV/c}$ the $\overline{p}/\pi^-$ ratio rises to $\simeq 0.4$ at $p_T \simeq 2\,\mathrm{GeV/c}$ and then drops, as expected if jet fragmentation is the dominant production mechanism for high p_T hadrons. The high p_T (anti)proton/pion ratios observed at RHIC are of the order of 1 which is much larger than in hadron-hadron collisions.

Different theoretical explanations have been proposed to describe such behavior. It has been suggested that hydrodynamic expansion alone or combined with hadronic re-scattering is responsible for the baryon dominance at high p_T [4,5,18,19]. Protons/anti-protons produced via a baryon junction mechanism combined with jet-quenching in the pion channel are shown to exhibit the same effect [7]. Intrinsic p_T broadening in the partonic phase caused by gluon saturation expected in high-density QCD [6] gives yet another alternative explanation.

To quantify the centrality and mass dependencies of hadron production, we determine the first moment ($<p_T>$ shown in Fig. 2) and the integral (dN/dy shown in Fig. 3) of the p_T distributions. Both quantities require extrapolation of the spectra below and above the measured range. For each particle species, we use several functional forms consistent with the data, as outlined above. The fraction of the yield in the extrapolated regions is estimated $30\pm6\%$ for pions, $40\pm8\%$ for kaons and $25\pm7.5\%$ for (anti)protons. Combining systematic uncertainties in the extrapolation fractions and the estimated background under mass-squared peaks (2%, 5% and 3%) yield systematic uncertainties in the measured $<p_T>$ of 7%, 10% and 8% for pions, kaons and (anti)protons, respectively. Further combining the above uncertainties, which only affect the shape of the spectra, with the 11% uncertainty in the absolute normalization gives systematic uncertainties of 13%, 15% and 14% in the measured dN/dy for pions, kaons and (anti)protons, respectively. We note that after converting to $dN/d\eta$, the sum of the identified charged hadron yields agrees with the previously published PHENIX results on total charged multiplicity $dN_{ch}/d\eta$ [1] within 5%.

Fig. 2 shows the $<p_T>$ as a function of N_{part} for π^+, K^+, p (left panel) and $\pi^-, K^-, \overline{p}$ (right panel). The full points are the PHENIX measurement, while the open points at $N_{part} = 2$ are interpolations to $\sqrt{s} = 130\,\mathrm{GeV}$ obtained from pp and $p\overline{p}$ data at lower [16] and higher energies [17], respectively. In peripheral Au-Au collisions at RHIC pions and kaons exhibit similar $<p_T>$ to those in pp collisions, but protons and anti-protons have significantly higher $<p_T>$, indicating that nuclear effects are important even at small N_{part}. For all measured particles species, the $<p_T>$ increases by $\approx 12-14\%$ from the first to the second centrality bin (i.e. N_{part} 14 to 79). Above $N_{part} = 100$ the pion and kaon $<p_T>$ appear to saturate, whereas the p and $\overline{p}$ $<p_T>$ rises slowly. However, we note that going from peripheral to the most central event class the overall increase in $<p_T>$ is $\approx 20 \pm 5\%$ independent of particle species.

The yields per participant as a function of N_{part} are shown in Fig. 3. The error bars include statistical and multiplicity dependent systematic errors. The systematic uncertainties in N_{part} that can move all curves independent of mass are shown with bands around the positive hadron points. The total systematic uncertainties in N_{part} and the yields at each N_{part} are listed in Table I.

For all particle species, the yield per participant increases with N_{part}. As in the $<p_T>$, most of the increase occurs between the two most peripheral centrality selections (i.e. N_{part} 14 to 79). However, unlike in the centrality dependence of the $<p_T>$, we see an indication that the total increase in the yields per participant differs among particle species as we go from peripheral to central events. The pion yield per participant rises by $21\% \pm 6\%(stat) \pm 8\%(syst)$. The kaon yields per participant rise faster than the pion yields: $94\% \pm 11\%(stat) \pm 26\%(syst)$ and $66\% \pm 12\%(stat) \pm 20\%(syst)$, for K^+ and K^-, respectively. Similar trends in the centrality dependence of strangeness production have been observed in lower energy heavy ion collisions at BNL-AGS [20,21] and at CERN-SPS [15]. It is interesting to note that at RHIC proton and anti-proton yields per participant behave similarly to the kaon yields and also rise faster than the pions with increasing N_{part}. The increase is $58\% \pm 5\%(stat) \pm 16\%(syst)$ and $72\% \pm 9\%(stat) \pm 20\%(syst)$, respectively. The similar centrality dependence in proton and anti-proton yields per participant indicates that baryon/anti-baryon pair production is the dominant source of protons and anti-protons alike.

In heavy ion collisions at AGS energies [23–25] the anti-proton production is close to threshold, the yields per participant are lower than in pp collisions and decrease from peripheral to central collisions. At SPS energies,

the anti-proton yield per participant is larger than the pp value and has almost no centrality dependence [26]. At RHIC, the total yield of anti-protons at mid-rapidity in central Au-Au collisions is a factor of $\simeq$ 1000 larger than at the AGS [23] and nearly an order of magnitude above that in Pb+Pb collisions at CERN [27]. Most of the increase is due to the $\sqrt{s}$ dependence of baryon/anti-baryon pair production, however the yield per participant rises noticably from peripheral to central collisions.

In conclusion, an intriguing new behavior in identified hadron production at RHIC is reported. In central Au-Au collisions the anti-protons yield is comparable to the negative pions at high p_T - a behavior never observed before in elementary or in heavy-ion collisions. Average p_T rises with centrality similarly for all particle species, while kaon, proton and anti-proton yields per participant increase faster than the pion yields.

We thank the staff of the RHIC project, Collider-Accelerator, and Physics Departments at BNL and the staff of PHENIX participating institutions for their vital contributions. We acknowledge support from the Department of Energy and NSF (U.S.A.), Monbu-sho and STA (Japan), RAS, RMAE, and RMS (Russia), BMBF, DAAD, and AvH (Germany), FRN, NFR, and the Wallenberg Foundation (Sweden), MIST and NSERC (Canada), CNPq and FAPESP (Brazil), IN2P3/CNRS (France), DAE and DST (India), LG-YF, KRF and KOSEF (Korea), and the US-Israel Binational Science Foundation.

---

* Deceased

† Not a participating Institution (author is an individual participant).

[1] K. Adcox *et al.*, Phys. Rev. Lett. **86**, 3500 (2001).
[2] K. Adcox *et al.*, Phys. Rev. Lett. **87**, 052301 (2001).
[3] B.B. Back *et al.*, Phys. Rev. Lett. **85**, 3100 (2000).
[4] D. Teaney *et al.*, Phys. Rev. Lett. **86**, 4783 (2001); nucl-th/0110037.
[5] P. Kolb *et al.*, Nucl. Phys. **A696**, 197 (2001); P. Huovinen *et al.*, Phys. Lett. **B503**, 58 (2001)
[6] J. Schaffner-Bielich *et al.*, nucl-th/0108048 and references therein.
[7] I. Vitev and Miklos Gyulassy, nucl-th/0104066.
[8] H. Hamagaki, *Proc. Quark Matter 2001, in press.*
[9] J. Velkovska, Proc. CAARI 2000, AIP **CP576**, 227 (2001).
[10] B.B. Back *et al.*, Phys. Rev. Lett. **87**, 102303 (2001).
[11] K. Adcox *et al.*,Phys. Rev. Lett. (in press); nucl-ex/0109003
[12] C. Albajar *et al.*, Nucl. Phys. **B335**, 261 (1990).
[13] L.Ahle *et al.*, Nucl. Phys. **A638**, 57c-68c (1998).
[14] I.G. Bearden *et al.*, Phys. Rev. Lett. **78**, 2080 (1997).
[15] J. Bachler *et al.*, Nucl. Phys. **A661**, 45c-54c (1999).
[16] B. Alper *et al.*, Nucl. Phys. **B100**, 237-290 (1975).
[17] T. Alexopoulos *et al.*, Phys. Rev. **D48**, 984 (1993).
[18] P. Huovinen *et al.*, hep-ph/0101136.
[19] W. Broniowski and W. Florkowski, nucl-th/0106050.
[20] L. Ahle *et al.*, Phys. Rev. **C59**, 2173 (1999).
[21] L. Ahle *et al.*, Phys. Rev. **C60**, 044904 (1999).
[22] J. Barrette *et al.*, Phys. Rev. Lett. **70**, 1763 (1993).
[23] L. Ahle *et al.*, Phys. Rev. Lett. **81**, 2650 (1998).
[24] D. Beavis *et al.*, Phys. Rev. Lett. **75**, 3633 (1995).
[25] M. Bennett *et al.*, Phys. Rev. **C56**, 1521 (1997).
[26] G. I. Veres, Nucl. Phys. **A661**, 383c-386c (1999).
[27] I.G. Bearden *et al.*, Phys. Lett. **B388**, 431-436 (1996).

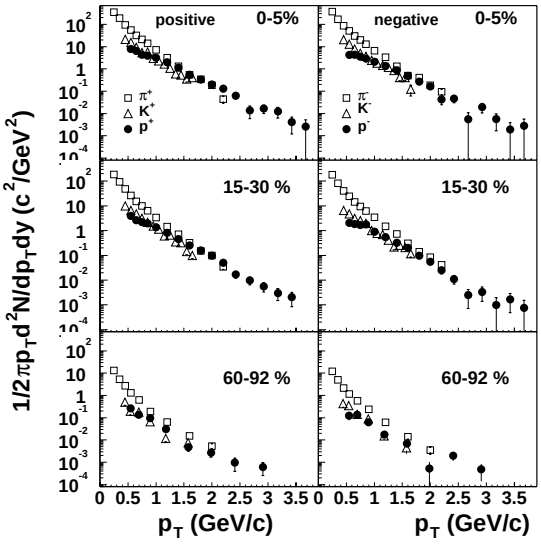

FIG. 1. Transverse momentum spectra measured at mid-rapidity for π^+, K^+, p (left) and $\pi^-, K^-, \overline{p}$ (right) at the three different centrality selections indicated in each panel. The symbols indicated in the top panels apply for all centrality selections.

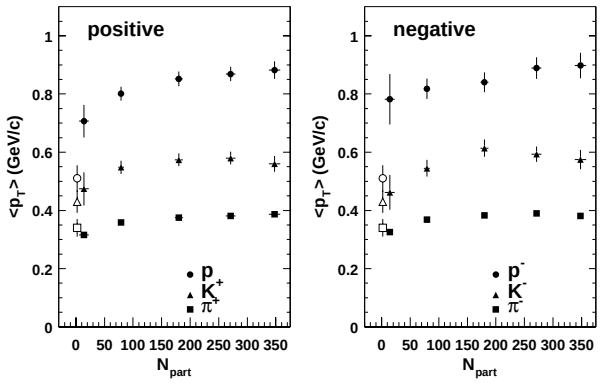

FIG. 2. Average transverse momentum for π^+, K^+, p (left) and $\pi^-, K^-, \overline{p}$ as a function of the number of nucleons participating in the collision N_{part}. The error bars represent the statistical errors. The systematic errors are discussed in the text. The open points are interpolations from pp and $p\overline{p}$ data, see text for details.

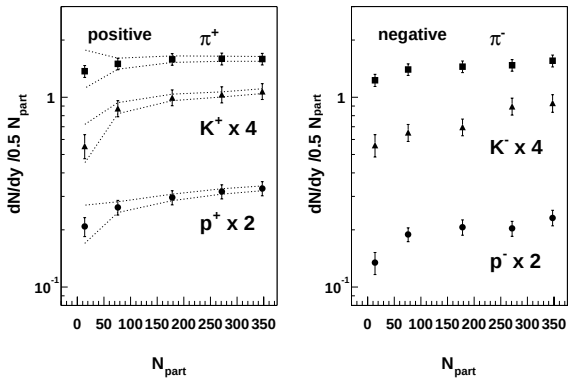

FIG. 3. $dN/dy_{|y=0}$ per participant for π^+, K^+, p (left) and $\pi^-, K^-, \overline{p}$ as a function of N_{part}. The error bars include statistical and systematic errors in dN/dy. The dashed lines around the positive hadrons show the effect of the systematic error on N_{part} which affects all curves in the same way.

TABLE I. Integrated hadron ($\pi^{\pm}, K^{\pm}$, and $p^{\pm}$) yields at mid-rapidity for five centrality classes (see text) identified by the indicated number of participants N_{part}. The errors on N_{part} are the systematic errors. The errors listed for $<dN/dy_{|y=0}>$ are statistical. The systematic errors are 13%, 15% and 14% for pions, kaons, (anti)protons, respectively.

N_{part}	348±10.0	271±8.4	180±6.6	79±4.6	14±3.3
π^+	276±3	216±2	141±1.5	57±0.6	9.6±0.2
π^-	270±3	200±2	129±1.4	53.3±0.6	8.6±0.2
K^+	46.7±1.5	35.0±1.3	22.2±0.8	8.3±0.3	0.97±0.11
K^-	40.5±2.3	30.4±1.4	15.5± 0.7	6.2±0.3	0.98±0.1
p	28.7±0.9	21.6±0.6	13.2±0.4	5.0±0.2	0.73±0.06
$\overline{p}$	20.1±1.0	13.8±0.6	9.2±0.4	3.6±0.1	0.47±0.05